SEMARAK ILMU PUBLISHING

Journal of Advanced Research in Fluid Mechanics and Thermal Sciences

Journal homepage:
https://semarakilmu.com.my/journals/index.php/fluid_mechanics_thermal_sciences/index
ISSN: 2289-7879

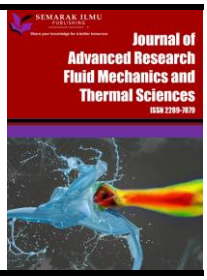

Experimental Study on Heat Transfer Characteristics of a ⊥-shaped Oscillating Heat Pipe Used in the Battery Thermal Management System

Lu Hongkun[1,2,*], Muhamad Mat Noor[1,♣], Ning Shuigen[2,3], Kumaran Kadirgama[1], Irfan Anjum Badruddin[4], Sarfaraz Kamangar[4]

[1] Faculty of Mechanical & Automotive Engineering Technology, Universiti Malaysia Pahang Al-Sultan Abdullah (UMPSA), Pekan, Pahang, Malaysia
[2] School of Automotive Engineering, Jiangxi Polytechnic University, Jiujiang 332000, Jiangxi, China
[3] Universiti Malaysia Pahang Al-Sultan Abdullah (UMPSA), Pekan, Pahang, Malaysia
[4] Mechanical Engineering Department, College of Engineering, King Khalid University, Abha 61421, Saudi Arabia

ARTICLE INFO

Article history:
Received 24 June 2024
Received in revised form 13 October 2024
Accepted 22 October 2024
Available online 10 November 2024

Keywords:
Oscillating heat pipe; heat transfer performance; filling ratio; binary mixture; thermal load

ABSTRACT

This paper introduces a ⊥-shaped oscillating heat pipe (OHP) with the purpose of improving the volumetric utilization of the battery thermal management system (BTMS) for electric vehicles. Distinguished from standard OHP structures, the evaporator and condenser sections of the ⊥-shaped OHP are oriented vertically in spatial arrangement. Experimental investigations were conducted on two types of ⊥-shaped OHPs and a standard OHP, employing filling ratios from 19.6% to 39.1%, working fluid mixtures of acetone with methanol, ethanol, and water, and thermal loads from 10 to 100W. The results indicate that all the OHPs with an acetone filling ratio of 26.1% exhibit minimum thermal resistance at 30W. When employing mixed working fluids, the acetone-ethanol and acetone-methanol combinations display the least and most temperature fluctuations, respectively. The OHP with mixed working fluids achieves no more improved thermal performance than the use of acetone. As the heating power increases, the operational stability of the ⊥-type OHP improves, however, the trend is opposite for the R-⊥-type OHP. In comparison to the standard OHP, the ⊥-type OHP demonstrates stronger oscillation stability at 100W and achieves a 3.3°C lower maximum temperature on the heat collector plate.

1. Introduction

Lithium-ion batteries, being the main source of energy for electric vehicles, offer significant performance advantages but release substantial heat throughout the charging and discharging procedures [1-3]. To increase the electric vehicle's driving range, researchers have continually sought to improve the volumetric utilization of power batteries and have developed battery structural designs such as Cell to Pack (CTP) and Cell to Chassis (CTC) [4-6]. Placing more lithium-ion battery

* *Corresponding author.*
E-mail address: maxlhk@163.com
♣ *Corresponding author.*
E-mail address: muhamad@umpsa.edu.my

https://doi.org/10.37934/arfmts.123.2.8298

packs within the limited space of the vehicle chassis exacerbates the heat generation from batteries, thereby imposing higher demands on battery thermal management system (BTMS). Improving the cooling efficiency, expanding the heat exchange surface areas while using the least amount of space have been the main challenges [7-9]. Air cooling, liquid cooling, phase-change material cooling, and heat pipe cooling are some of the popular battery cooling strategies used nowadays, while air and liquid cooling are commonly employed in the thermal management of electric vehicle batteries [7-18].

Despite their simple design, air cooling systems provide less consistent temperatures and reduced cooling effectiveness because air has weaker thermal qualities, such as density, thermal conductivity, and specific heat. Additionally, the system tends to be equipped with low-performance power battery packs and takes up more space [18,19]. In contrast, liquid cooling, compared to air cooling, typically offers higher heat transfer coefficients and cooling capacity, rendering it an indispensable choice for high-end automotive BTMS. However, liquid cooling is associated with the risk of fluid leakage and complex pipeline layout, resulting in higher costs and challenges in system maintenance and repair [20].

An innovative heat pipe called the oscillating heat pipe (OHP) was first put out by Akachi [21] in 1990. In comparison to conventional OHP, it features a smaller inner diameter and forms multiple randomly distributed vapor plugs and liquid slugs within the interior, driven by surface tension forces. When the evaporator and condenser sections of the OHP are subjected to heating and cooling, respectively, these vapor plugs and liquid slugs undergo cyclic oscillations, facilitating heat transfer through phase change and convective processes. The OHP offers advantages such as high heat transfer efficiency, simple structure, low cost, an exceptionally high heat dissipation limit, and long-distance heat transfer capability. In recent years, there has been a growing interest among scholars in applying OHP to enhance battery thermal management. However, in previous studies, batteries are often situated within the evaporator section of the OHP, sharing the same plane with the condenser and adiabatic sections [22-27].

The condenser section is only used to install the cooling device, which means that the volume utilization efficiency is very low. The condenser section primarily accommodates liquid-cooling or air-cooling heat dissipation modules, which have a limited range of functionality, occupy significant space, and pose challenges in lithium batteries arrangement. Consequently, current studies on BTMS with OHP have suffered from relatively low volumetric utilization rates of battery packs, hindering their practical applicability [28].

To address the shortcomings of existing BTMS utilizing the OHP, a novel BTMS based on a ⊥-shaped OHP is proposed. The parametric effects of filling ratios, mixture working fluids, and heat loads on the startup and operation performance of the three different type OHPs were investigated in the paper.

2. Structural Characteristic of BTMS based on ⊥-shaped OHP

When designing the BTMS for square-shaped batteries, coupling OHP with liquid cooling yields higher space utilization efficiency. This paper focuses on square lithium-ion batteries and aims to enhance the volumetric utilization of the BTMS. To achieve this goal, a liquid-cooling BTMS based on ⊥-shaped OHP is proposed. As illustrated in Figure 1, this system features a liquid cooling plate designed with an openable structure. The outer surfaces of the liquid cooling plate on both sides make direct contact with the battery cells for efficient heat dissipation, while the central portion is machined with circular channels that match the configuration of the OHP. The condenser section of the OHP, coated with thermally conductive silicone grease, is inserted into these circular channels,

effectively utilizing the liquid cooling plate for heat dissipation. The evaporator section of the OHP is oriented vertically to the condenser section. The evaporator section comes into touch with the bottom surfaces of the square battery cells through the aluminum heat collector plates, absorbing heat from these surfaces. The adiabatic section of the OHP is relatively short, primarily concentrated in the arc-transition region connecting the evaporator and condenser sections.

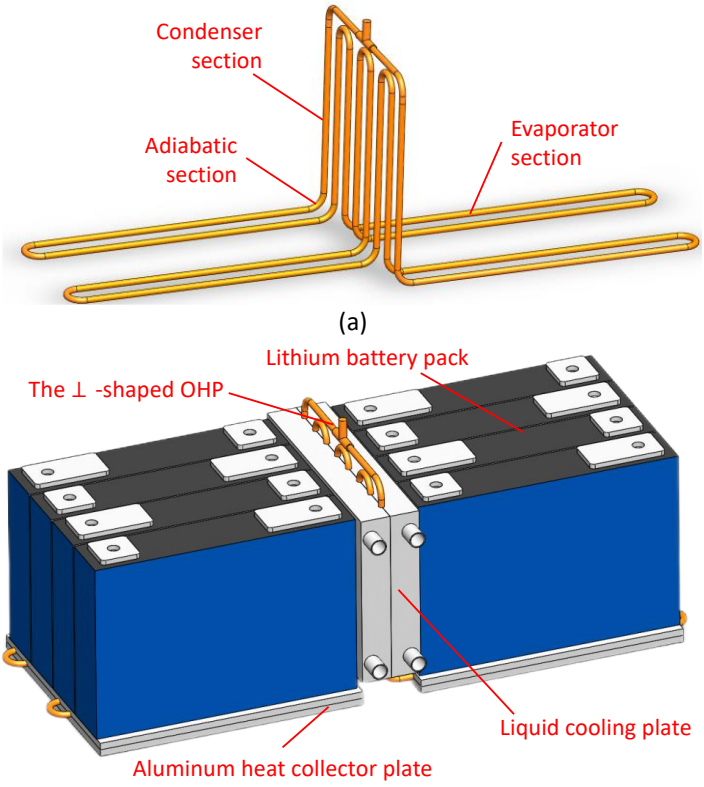

Fig. 1. Structural characteristics of BTMS based on ⊥-shaped OHP; (a) The ⊥-shaped OHP, (b) The battery pack space layout

Without increasing the number of liquid cooling plates, this new BTMS allows the heat generated by the batteries to be dissipated either through direct contact between the battery pack and the liquid cooling plate or via heat transfer through the OHP. This design essentially expands the heat exchange surface area of the battery, presenting the potential to reduce the maximum battery temperature and enhance the temperature uniformity of the battery pack. Furthermore, the lengths of the evaporator and condenser sections of the OHP within the BTMS can be flexibly adjusted according to the structural size of the square-shaped power batteries, rendering it highly adaptable.

3. Experimental Device and Data Processing

The experimental setup, illustrated in Figure 2, is a closed-loop system comprising mainly a ⊥-shaped structure OHP, a simulated heat source, a cooling system, a data collection system, and related pipelines components. To reduce heat dissipation losses from the evaporator section to the surrounding environment, the system employs aluminum foil insulation to thermally insulate the experimental setup. In the experiment, a VC2060H signal generator is used to manage the flow of cooling fluid within the water pump, while an MS10030D DC power supply powers the heat source.

It's crucial to remember that the focus of the study is on the heat transfer performance of the⊥-shaped OHP. In the experiments, the metal heating films, which are affixed to the heat-collecting plates in the evaporator section and are encased in a polyimide substance, supply the input heat to the OHP. Therefore, there is no direct contact between the heat source and the liquid cooling plate, and the heat generated by the battery pack can only be transferred through the ⊥-shaped OHP. Temperature signals are collected using Agilent 34970A and PT100 thermocouples with a data acquisition interval of 1 second.

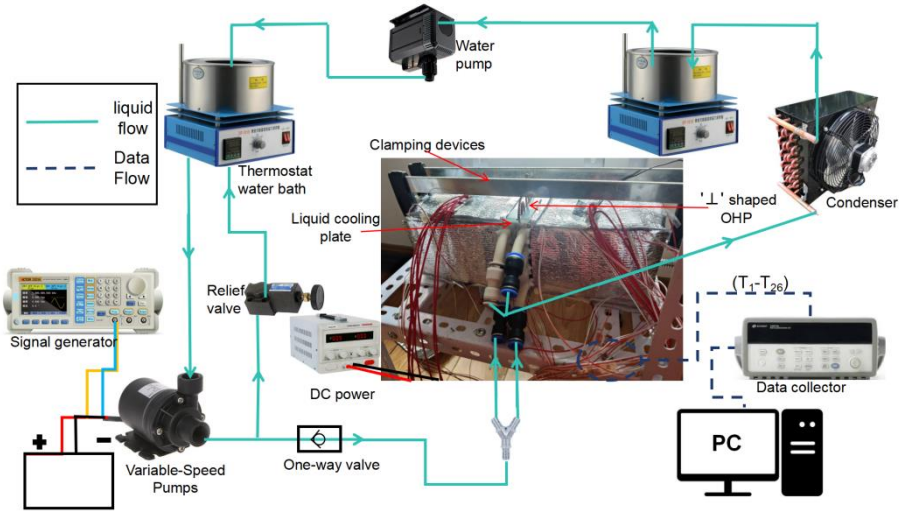

Fig. 2. Schematic diagram of the test bench

3.1 Experimental Subjects

The study focuses on a 51A·h square-shaped lithium-ion battery with dimensions measuring 148mm × 26mm × 97mm. The copper OHP used in the experiments primarily has the following dimensions: an exterior diameter of 3mm, an interior diameter of 2mm, equipped with 4 elbows, each with a radius of 7mm. The straight portion of the evaporator section measures 148mm in length, while the straight segment length of the condenser section is 97mm. Gravity exerts a significant influence on the flow of the working fluid within OHP [29,30]. For conventional OHP, as illustrated in Figure 3(a) and referred to as C-type OHP, the evaporator, adiabatic, and condenser sections are all located in the same plane, and the condenser section is positioned above while the evaporator section is located below, facilitating the flow of the working fluids within the OHP through the influence of gravity.

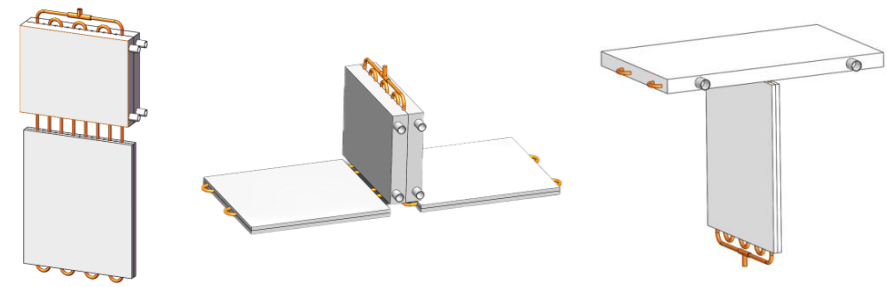

(a) C-type OHP (b) ⊥-type OHP (c) R-⊥-type OHP

Fig. 3. Experimental pulsation heat pipe structure diagram

Two alternative designs for the ⊥-shaped OHP exist, both of which adhere to the spatial distribution design idea of placing the evaporator portion below and the condenser section above. According to Figure 3(b) and Figure 3(c), these are the two structural variations of ⊥-shaped OHPs. The structure with a vertically oriented condenser section is denoted as the ⊥-type OHP, while the one with a horizontally arranged condenser section is referred to as the R-⊥-type OHP.

Temperature measurement points are consistently distributed across the OHPs of different structures. As depicted in Figure 4, T1 to T8 (with a diameter of 0.1mm and an accuracy of ±0.2°C) are temperature measurement points distributed on either side of the evaporator section. T9 to T16 are located at both ends of the condenser section. Additionally, five temperature measurement points are individually arranged on each heat-collecting plate. Experimental tests are conducted on the two types ⊥-shaped OHPs and a conventional OHP, which serves as the control group. The experiments are carried out at a 25°C standard temperature, with the cooling water temperature held constant at 25°C. The goal of the study is to investigate the impact of the various mixed working fluids (acetone with methanol, ethanol, and water), the filling ratios (19.6%, 26.1%, 32.6%, 39.1%), and the heating power loads (10–100W) on the heat transfer performance of the ⊥-shaped OHPs.

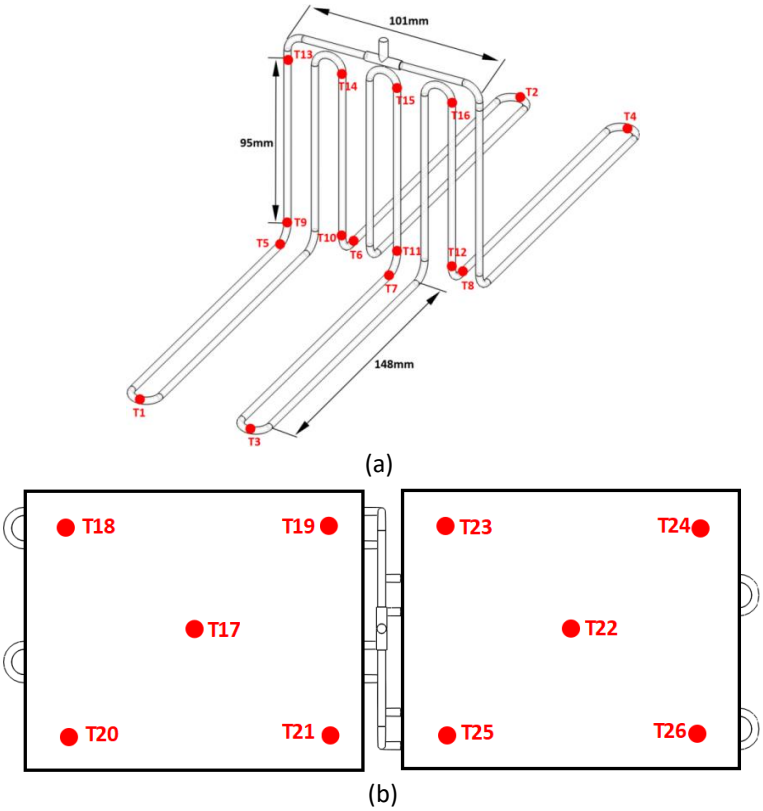

Fig. 4. Distribution of thermocouple temperature measurement points of (a) the OHP, (b) heat collector plates

3.2 Experimental Error Analysis

As shown in Eq. (1), thermal resistance *R* is employed to assess the heat transfer performance of the OHP. In the equation, T_{eva} and T_{con} denote the average wall temperatures of the evaporator and condenser sections, respectively. *Q* represents the heating power applied to the evaporator section. The average wall temperatures of the evaporator and condenser sections in the OHP can be expressed using Eq. (2) and Eq. (3), respectively.

$$R = \frac{T_{eva} - T_{con}}{Q} \tag{1}$$

$$T_{eva} = \frac{1}{8}\sum_{i=1}^{8} T_i \tag{2}$$

$$T_{con} = \frac{1}{8}\sum_{i=9}^{16} T_i \tag{3}$$

The primary sources of error in the experiment stem from the temperature data collected during the experimental process and the heating data from the power supply. Additionally, related parameters, when calculated using equations, can lead to greater computational errors, which can be quantified using Eq. (4) [31]

$$\frac{\Delta \mathbf{y}}{y} = \sqrt{\sum_{i=1}^{n} \left(\frac{\Delta \mathbf{x}_i}{x_i}\right)^2} \tag{4}$$

where $\Delta x_i/x_i$ represents the measurement error associated with the indirect error $\Delta y/y$. The errors associated with the heat source and thermal resistance can be calculated using Eq. (5) to Eq. (6).

$$\frac{\Delta Q}{Q} = \sqrt{(\frac{\Delta U}{U})^2 + (\frac{\Delta I}{I})^2} \tag{5}$$

$$\frac{\Delta R}{R} = \sqrt{(\frac{\Delta T_{eva}^2 + \Delta T_{con}^2}{T_{eva} - T_{con}})^2 + (\frac{\Delta Q}{Q})^2} \tag{6}$$

During the heating tests of the OHP's evaporator section, the heat pipe was enveloped with well-insulating thermal insulation. Additionally, considering the precision of the testing apparatus and following the principles of error propagation, the relative error of thermal resistance R can be determined using Eq. (5) to Eq. (6). After calculations, the computed errors for the relevant parameters are presented in Table 1.

Table 1
Experimental uncertainties of main parameters

Parameters	Uncertainty (%)
T_i (i=1,2⋯26)	±0.3%
T_{max}	±0.3%
Q	3.2%
R	3.8%

4. Results and Discussion

4.1 Thermal Effect of the Filling Ratios on ⊥-shaped OHP

The filling ratio (FR) directly determines the total quantity of working fluid within the OHP, exerting a substantial impact on the performance of the OHP [32-34]. With acetone as the working fluid and 30W of heating power, Figure 5 shows temperature curves at the evaporator section measurement point T2 for various structural OHPs under varied fill ratios. Figure 6 illustrates how the thermal resistance of the OHPs varies under the corresponding circumstances.

In summary, it is observed that both the C-type OHP and the two types of ⊥-shaped OHPs exhibit the lowest evaporator section temperatures and the optimal heat transfer performance while the fill

ratio is set at 26.1%, which the average thermal resistance of the ⊥-type OHP approaches 0.283°C/W, similar to that of the C-type OHP. However, the R-⊥-type OHP reveals more pronounced vibrations, with magnitudes varying from 32.4°C to 39.5°C, and a thermal resistance of 0.385°C/W. At a filling ratio of 19.6%, the insufficient working fluid within the OHP led to ineffective moistening of the evaporation section. During the experimental process, neither ⊥-type nor R-⊥-type OHPs displays the sustained and distinct temperature oscillations, indicating the absence of startup in the OHPs. The heat transfer form in the OHPs is purely conductive, resulting in almost identical thermal resistances, approximately 1.17°C/W. Conversely, The C-type OHP can startup and operate at a filling ratio of 19.6%. This is due to the evaporator and condenser sections being on the same plane, allowing for better utilization of gravity as a driving force. However, due to the limited working fluid and acetone's high vaporization tendency, the C-type OHP exhibits significant temperature fluctuations, reaching 6.3°C, in its steady-state operation.

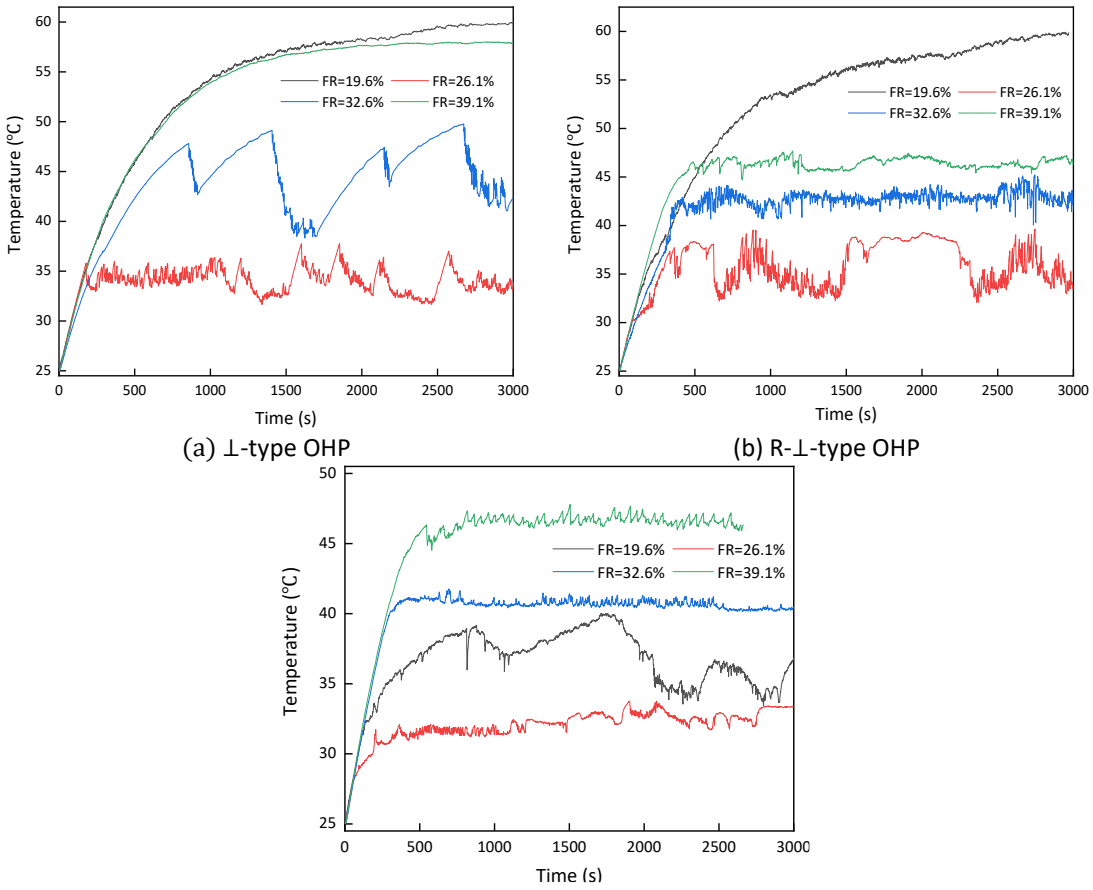

(a) ⊥-type OHP (b) R-⊥-type OHP

(c) C-type OHP

Fig. 5. Temperature curves of three type OHPs under different filling ratios

As the filling ratio increases from 26.1% to 39.1%, both the R-⊥-type OHP and the C-type OHP, which have vertically oriented evaporator sections, present similar trends. The fluid's internal shear stress progressively increases as the filling ratio rises. When the OHP operates steadily, the performance of heat transfer somewhat decreases and the stable temperature in the evaporator portion rises. On the other hand, the amplitude of the temperature oscillation reduces, improving pulsation flow stability. Notably, at a filling ratio of 39.1%, the heat transfer performance of the R-⊥-type OHP slightly surpasses that of the C-type OHP, with respective average thermal resistances of 0.716°C/W and 0.723°C/W. Conversely, as the filling ratio increases, the ⊥-type OHP, with the horizontally oriented evaporator section, accumulates more working fluid within the evaporator

section during startup stage. This results in increased resistance between the working fluid and the inner wall during the flow process, making it more challenging for the ⊥-type OHP to start normally. Consequently, at a filling ratio of 32.6%, the ⊥-type OHP exhibits intermittent operation with significant fluctuations in the temperature range of 38.4-49.1°C, resulting in an increased average thermal resistance of 0.63°C/W. When the filling ratio reaches 39.1%, the ⊥-type OHP is no longer able to startup successfully under a 30W heat source.

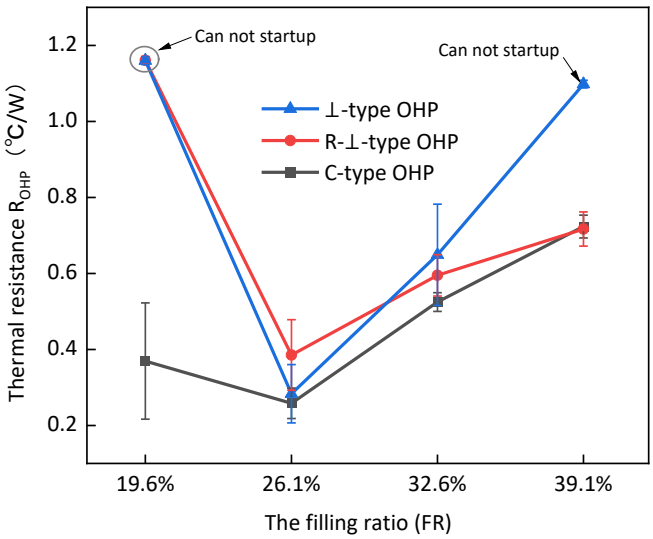

Fig. 6. Thermal resistance changes of three type OHPs under different filling ratios

4.2 Thermal Effect of the Mixed Working Mediums on ⊥-shaped OHP

The working fluid's physical characteristics are closely related to the thermodynamic performance of the OHP [35-38]. Commonly used working fluids for OHP include water, ethanol, methanol, and acetone. The physical properties of these fluids (all values are theoretical values at 25°C and standard pressure) are presented in Table 2. Compared to other working fluids, acetone demonstrates a higher $(dP/dT)_{sat}$, signifying that the evaporator and condenser sections can generate a significant pressure differential with a smaller temperature variance. This facilitates the movement of the working fluid within the OHP. Additionally, the lower latent heat of acetone is more conducive to the generation and rupture of vapor bubbles. Hence, acetone, in this part of experiments, was chosen as the primary working fluid.

As illustrated in Figure 7, while using a 30W heater with a 26.1% filling ratio, the temperature curves at evaporator section point T2 are investigated for different acetone-based working fluids: pure acetone, acetone-methanol (2:1 volume ratio), acetone-ethanol (2:1 volume ratio), and acetone-water (2:1 volume ratio), across various types of OHPs.

Table 2
Working substance property of different working mediums

Working medium	T_{sat} (℃)	ρ_l (kg/m^3)	H_{fg} (kJ/kg)	σ (N/m)	μ (mPa·s)	$(dP/dT)_{sat}$ (kPa/K)	λ_1 (W/m·K)
water	100	998	2258	0.0728	1.01	0.14	0.599
methanol	64.5	805	1102	0.0226	0.58	0.36	0.217
ethanol	78.3	809	846	0.0228	1.19	0.35	0.172
acetone	56.2	757	523	0.0237	0.32	1.15	0.178

In Figure 7(a), which represents the acetone-methanol mixed working fluid, the initiation temperature for the R-⊥-type OHP is 54.9℃, exceeding that of the C-type and ⊥-type OHPs at 41.7℃ and 45℃, respectively. This difference arises due to the horizontal orientation of the condenser section in the R-⊥-type OHP, consequently, the low-temperature liquid working fluid in the condenser section cannot rely on gravity as a driving force when flowing towards the evaporator section. As a result, a higher-pressure difference is required for the initiation of the R-⊥-type OHP. Moreover, the R-⊥-type OHP demonstrates fluctuations within a considerable temperature range of 57-70℃ during steady-state operation.

This phenomenon is attributed to the horizontal arrangement of the condenser section, causing an "accumulation" effect where the liquid working fluid adheres to the horizontal pipe wall of the condenser section. Only when the temperature reaches a sufficiently high level and is driven by a significant pressure differential, does the accumulated low-temperature liquid working fluid rapidly propel towards the evaporator section. Consequently, the temperature in the evaporator section rapidly decreases, perpetuating this cyclic process and resulting in the observed fluctuations within the broader temperature range. Once the ⊥-type OHP is started, it initially keeps oscillating steadily in the 45℃ around. But after 1945 seconds, isolated dry-out events show up, and the temperature eventually reaches 60℃. This is due to the horizontal arrangement of the evaporator section in the ⊥-type OHP, which hinders the passage of low-temperature liquid working fluid into the evaporator section's bottom area.

Figure 7(b) employs an acetone-ethanol hybrid working fluid. In comparison to methanol, ethanol exhibits a higher boiling point and a smaller $(dP/dT)_{sat}$ at the same temperature and pressure conditions. Consequently, within the same OHP structure, the initiation time using the acetone/ethanol hybrid working fluid is later compared to acetone/methanol, corresponding to a higher temperature. Taking the R-⊥-type OHP as an example, its initiation temperature is 60.1℃, with an initiation time of 820 seconds, which is 5.2℃ higher and delayed by 211 seconds compared to acetone/methanol mixtures. It is noteworthy that due to the formation of a non-azeotropic solution with acetone/ethanol mixtures, the vaporization of ethanol is suppressed, effectively preventing localized dry-out in the evaporator section of the OHP. Under the condition of acetone/ethanol mixtures, the steady-state temperature of the C-type OHP is 44.7°C, exhibiting minimal fluctuations. Conversely, in both the ⊥-type and R-⊥-type OHPs, the stability of temperature fluctuations is enhanced with acetone/methanol mixtures, which the corresponding stable temperature ranges are 52.4-58.9°C and 53.5-61°C, respectively.

The acetone-water working mixed fluid is used in Figure 7(c). The ⊥-type and C-type OHPs have initiation temperatures of 50.2°C and 43.6°C, respectively. Compared to utilizing the acetone/ethanol mixes, the temperatures are lower. This is because acetone/water mixtures also form non-azeotropic solutions, where the characteristics on suppression of phase change cause most of the water in the mixture to remain in the liquid phase. The liquid-phase water has a significantly higher energy-carrying capacity than ethanol, and water also possesses lower dynamic viscosity, resulting in reduced flow resistance and a lower startup temperature. Similar to acetone/methanol mixtures, the ⊥-type OHP experiences localized dry-out after initiation, occurring at 934 seconds. However, as the temperature rises to 60°C, the ⊥-type OHP resumes the flow, with liquid-phase working fluid from the condenser section returning to the evaporator section. With lowering the evaporator section's temperature, a new steady state is established.

In Figure 7(d), acetone as a single working fluid is utilized. Compared to the other working fluids used in the experiment, acetone possesses the lowest boiling point, the largest $(dP/dT)_{sat}$ value, and the smallest dynamic viscosity. Consequently, The OHP with acetone is more prone to initiation, leading to easier vaporization and nucleate boiling, resulting in more pronounced oscillations after

initiation. Under acetone as the working fluid, differences in heat pipe structure have minimal impact on the initiation time, with C-type, ⊥-type, and R-⊥-type OHPs corresponding to initiation times of 179 seconds, 187 seconds, and 220 seconds, sequentially. Following the initiation, the R-⊥-type OHP exhibits the most significant temperature oscillations during steady-state operation, with vigorous fluctuations in the range of 32.1-39.5°C. Subsequently, the ⊥-type OHP and the C-type OHP display oscillations with amplitudes of 31.8-37.8°C and 31.2-33.8°C, respectively.

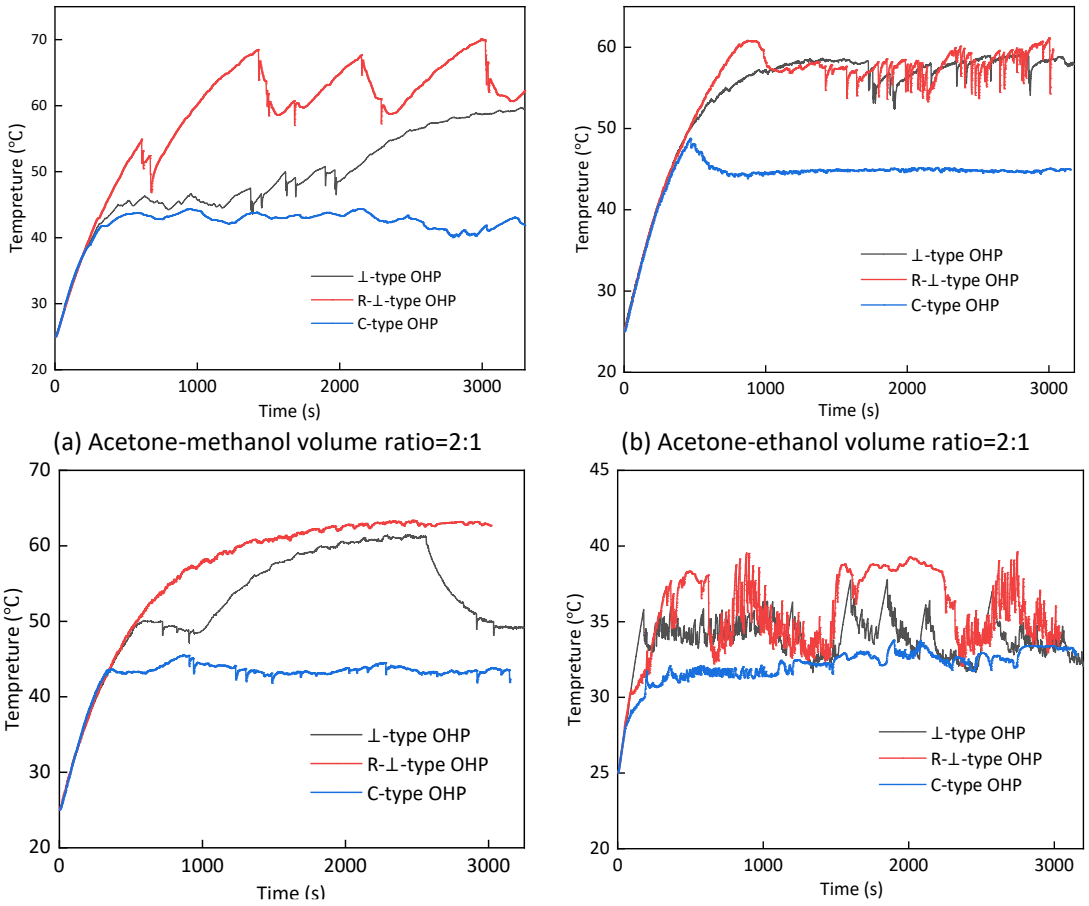

(a) Acetone-methanol volume ratio=2:1 (b) Acetone-ethanol volume ratio=2:1

(c) Acetone-water volume ratio = 2:1 (d) Acetone

Fig. 7. Temperature curves of three type OHPs under different mixed working fluids (T2)

In summary, at a heating power of 30W, the evaporator temperatures in T2 of various acetone-based mixed working fluids are higher than that of pure acetone, which means the mixed working fluids did not exhibit an obvious advantage over pure acetone. The structural design of the OHP has a significant influence on the startup and steady-state performance. The evaporator section of the C-type OHP is positioned at the top, while the condenser section is at the bottom, both situated in the same vertical plane, where gravity plays a role as one of the driving forces for the OHP. However, in the ⊥-shaped OHP, the evaporator and condenser sections are spatially oriented perpendicularly. This implies that either the evaporator or condenser section of ⊥-shaped OHPs is arranged horizontally, which, to some extent, is not conducive to utilizing gravity to facilitate the movement of the working fluid within the OHP. This adverse effect becomes more pronounced once the heat power is smaller.

4.3 Thermal Effect of the Heating Powers on ⊥-shaped OHP

In the experimental investigations of the influence of heating powers on the thermal performance of the ⊥-shaped OHPs, acetone was employed as the working fluid, with a constant fill ratio of 26.1%. As illustrated in Figure 8, at heating power levels ranging from 10 to 60W, the temperature curves are recorded at T2, T10 and T17 for two type ⊥-shaped OHPs, which these three temperature measurement points are located, subsequently, in the evaporator section, condenser section, and heat collection plate.

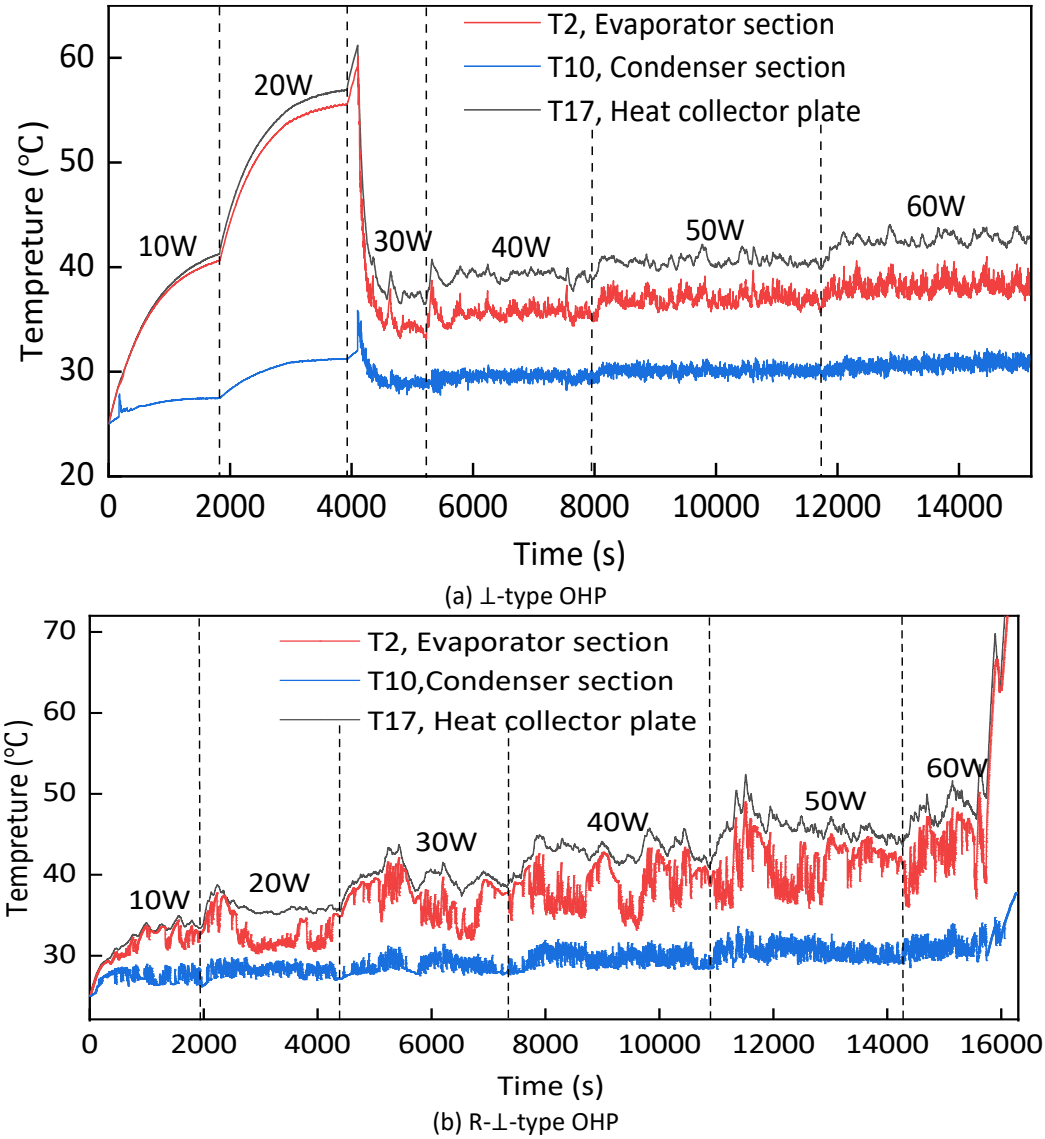

Fig. 8. Temperature curves of ⊥-shaped OHPs under different heating powers (10-60W)

In Figure 8(a), due to insufficient heating power, at 10-20W, the ⊥-type OHP encounters a failure to initiate, resulting in minimal temperature disparity between the evaporator section and the heat collection plate. However, as T2 increases to 60°C with the heating output reaches 30W, the ⊥-type OHP initiates, and a substantial volume of low-temperature liquid working fluid, previously accumulated in the condenser section, quickly flows into the evaporator section to absorb heat. Within just 10 seconds, both the evaporator section and the collector plate at T2 and T17 experience a significant decrease in temperature to 35°C. Simultaneously, the work fluid flowing from the

evaporator section to the condenser section rapidly raises the temperature at point T10 in the condenser section from 32.0°C to 35.9°C. Subsequently, the oscillations within the ⊥-type OHP stabilize. With further increases in heating power, temperatures at the measurement points in the heat collection plate, evaporator, and condenser sections of the ⊥-type OHP gradually rise, resulting in more stable temperature fluctuations.

In contrast, as seen in Figure 8(b), the R-⊥-type OHP successfully initiates at 10-20W, but experiences significant fluctuations in the temperature of the evaporator section. The stability of the R-⊥-type OHP does not exhibit significant improvements as the heating power increases and the fluid motion repeats a pattern of "intense oscillation-stagnation". Ultimately, dry-out occurs at 60W, resulting in a rapid temperature increase.

As depicted in Figure 9, temperature curves at the evaporator section T2 and the heat collection plate T17 during different heating power levels are presented for both C-type and ⊥-type OHPs. For every power level, the curve shows a steady state running time of 20 minutes. Overall, Within the 10-100W range, the C-type OHP functions normally. Temperatures rise in the evaporator portion and collection plate as power increases. At 100W, the heat collection plate reaches its highest temperature, reaching 59.3°C, which already approaches the upper safety limit for the operational temperature of the battery. In the bottom right corner of Figure 9, temperature curves for the evaporator section and heat collection plate of the ⊥-type OHP are provided with the power range of 70-100W.

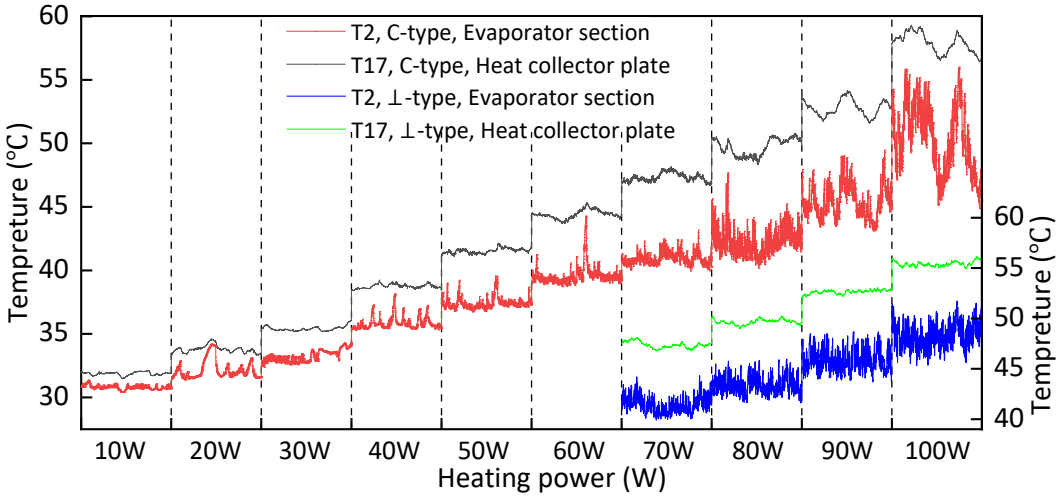

Fig. 9. Temperature curves of C-type and ⊥-type OHPs under different heating powers

It is noteworthy that the temperature fluctuation in the evaporator section of the C-type OHP intensifies with the increase in heating power. In contrast, the temperature fluctuation in the evaporator section of the ⊥-type OHP exhibits stronger stability. This difference is also reflected in the heat collection plate temperature fluctuations; at 100W, the highest temperature in the collector plate at T17 of the ⊥-type OHP reaches 55.9℃, which is 3.4°C lower than that of the C-type OHP.

Figure 10 illustrates the temperature frequency distribution of 2000 consecutive temperature points at T2 during steady-state operation for both the ⊥-type and C-type OHPs at heating power levels of 70W and 100W. As shown in the figure, at a heating power of 70W, the temperature frequency distribution for the ⊥-type OHP closely resembles that of the C-type OHP, with slightly more temperature points clustered around the left side of the mean temperature. The temperature points for both ⊥-type and C-type OHPs fall within the range of 46.7-48.1°C, and their average temperatures exhibit minimal differences, measuring 47.4°C and 47.3°C, correspondingly.

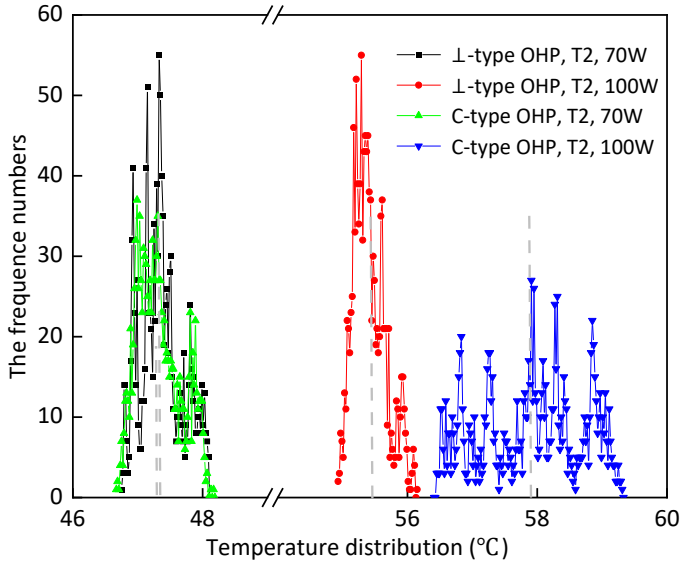

Fig. 10. Temperature frequency distribution of C-type and ⊥-type OHPs (70W and 100W)

However, utilizing a 100W heater, the average temperature for the ⊥-type OHP rises to 55.4°C. Nevertheless, the shape of the temperature frequency distribution remains relatively consistent with that observed at 70W, indicating a strong oscillation stability for the ⊥-type OHP. In contrast, at the heating power of 100W, the temperature frequency distribution for the C-type OHP undergoes significant changes in its shape, transitioning from a "tall and slim" distribution to a "short and wide" one. This transformation suggests increased temperature fluctuations and greater dispersion of temperature points. Meanwhile, the average temperature for the C-type OHP rises to 57.9°C, with a temperature range between 56.5°C-59.3°C. Additionally, the frequency of temperature points near the mean temperature decreases from around 35 to approximately 25.

Figure 11 illustrates the thermal resistance curves for different OHPs at various power levels. Due to the utilization of acetone as the working fluid with a filling ratio of 26.1%, under stable operating conditions, the thermal resistance of all types of OHPs remains below 0.9°C/W. The average thermal resistance for R-⊥-type OHP and C-type OHP at 10W are 0.67°C/W and 0.58°C/W. With increasing the heat power load, the thermal resistance of the OHPs rapidly decreases. The lowest thermal resistance values for ⊥-type and C-type OHPs are observed around 60-70W. Notably, for ⊥-type OHP, once the heating power reaches 60W, there is minimal variation in thermal resistance with the heat power levels growing, with average values hovering around 0.23°C/W. Conversely, C-type OHP demonstrates its lowest average thermal resistance at 70W, measuring 0.228°C/W. As the heat power loads continue to rise, temperature oscillations intensify for C-type OHP, resulting in an enlargement of the thermal resistance's fluctuation range. When the heat load reaches 100W, the thermal resistance fluctuates within the range of 0.199-0.311°C/W.

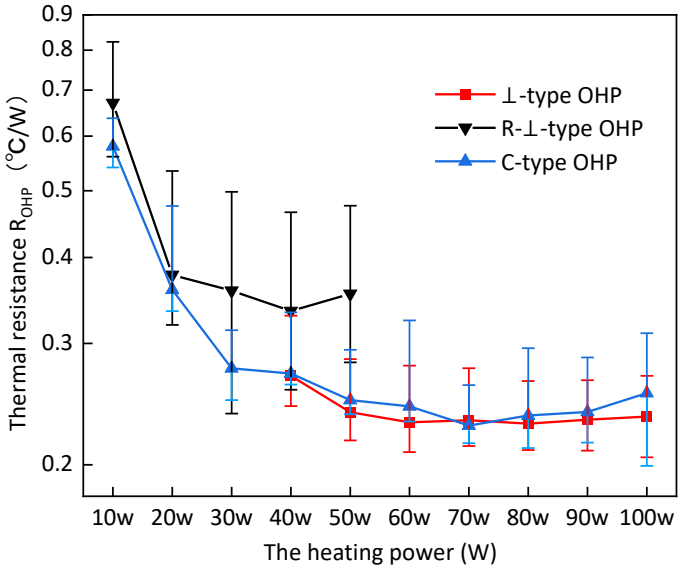

Fig. 11. The thermal resistance curves of three type OHPs under different heating powers

5. Conclusion

Based on the proposed structural characteristics of the ⊥-shaped OHP for the liquid-cooling BTMS, this study conducted experiments on the ⊥-type OHP, R-⊥-type OHP, and a control group of C-type OHP. The aim was to investigate the heat transfer performance of the ⊥-shaped OHPs under various filling ratios, working fluids, and heating powers. The conclusions drawn are as follows

i. Using acetone as the working fluid and under 30W, the lowest evaporator section temperatures for all types of OHPs occur at a filling ratio of 26.1%. As the filling ratio increases, both R-⊥-type and C-type OHPs experience higher startup temperatures and improved oscillation stability. In the case of the ⊥-type OHP, at a filling ratio of 32.6%, the working fluid inside the OHP exhibits intermittent operation, with significant fluctuations occurring within the temperature range of 38.4-49.1°C. As the filling ratio continues to increase to 39.1%, the ⊥-type OHP becomes unable to startup.

ii. At a filling ratio of 26.1% and a heat load of 30W, compared to acetone as working fluid, OHPs using hybrid working fluids show no significant enhancements in terms of heat transfer performance. The acetone-ethanol mixed working fluid forms a non-azeotropic solution, resulting in the smallest temperature oscillation intensity in the evaporator section among the three types OHPs. Conversely, the acetone-methanol hybrid working fluid, due to the ease of methanol vaporization and the formation of dry-out regions in the evaporator section, exhibits the largest temperature oscillation amplitude.

iii. With the acetone filling ratio of 26.1%, the ⊥-type OHP experiences failure to initiate at 10-20W, however, as the heat power increases, the operational stability of the ⊥-type OHP improves. At 70-100W, the temperature oscillation stability in the evaporator section of the ⊥-type OHP surpasses that of the C-type OHP. At 100W, the highest temperature in the heat collector plate of the ⊥-type OHP is 3.3°C lower than that of the C-type OHP. As for the R-⊥-type OHP, it appropriately initiates at 10-20 W. However, even with this increased heating power, the stability of the R-⊥-type OHP is not enhanced, and it experiences dry-out at 60W.

Credit Authorship Contribution Statement

Lu Hongkun Investigation, Formal analysis Methodology and Writing original draft; M.M. Noor Conceptualization, Validation, Writing - reviewing & editing, Supervision and Resources; Ning Shuigen Visualization, Formal analysis, and Writing - reviewing & editing, K. Kadirgama Supervision and Writing - reviewing & editing; I. A. Badruddin Conceptualization, Writing - reviewing & editing, Supervision and Resources; S. Kamangar Writing - reviewing & editing, Supervision and Resources.

Declaration of Competing Interest

The authors declare that the work reported in this study was not affected by any conflicting financial interests or personal connections.

Data Availability

No data was used for the research described in this article.

Acknowledgement

The financial support bythe Scientific and Technological Research Project for Education Department of Jiangxi Province (GJJ2404911), the Ministry of Higher Education, Malaysia through the Fundamental Research Grant Scheme: FRGS/1/2024/TK10/UMP/02/15 and Universiti Malaysia Pahang Al-Sultan Abdullah (RDU240117). The support for the laboratory used from Jiangxi Polytechnic University, China and Universiti Malaysia Pahang Al-Sultan Abdullah was equally acknowledged and appreciated

References

[1] Choudhari, V. G., A. S. Dhoble, and T. M. Sathe. "A review on effect of heat generation and various thermal management systems for lithium ion battery used for electric vehicle." *Journal of Energy Storage* 32 (2020): 101729. https://doi.org/10.1016/j.est.2020.101729

[2] Kong, Depeng, Hongpeng Lv, Ping, and Gongquan Wang. "A review of early warning methods of thermal runaway of lithium ion batteries." *Journal of Energy Storage* 64 (2023): 107073. https://doi.org/10.1016/j.est.2023.107073

[3] Shahid, Seham, and Martin Agelin-Chaab. "A review of thermal runaway prevention and mitigation strategies for lithium-ion batteries." *Energy Conversion and Management: X* 16 (2022): 100310. https://doi.org/10.1016/j.ecmx.2022.100310

[4] Jin, Changyong, Yuedong Sun, Jian Yao, Xuning Feng, Xin Lai, Kai Shen, Huaibin Wang et al. "No thermal runaway propagation optimization design of battery arrangement for cell-to-chassis technology." *ETransportation* 14 (2022): 100199. https://doi.org/10.1016/j.etran.2022.100199

[5] Khan, F. M. Nizam Uddin, Mohammad G. Rasul, A. S. M. Sayem, and Nirmal K. Mandal. "Design and optimization of lithium-ion battery as an efficient energy storage device for electric vehicles: A comprehensive review." *Journal of Energy Storage* 71 (2023): 108033. https://doi.org/10.1016/j.est.2023.108033

[6] Chen, Siqi, Guangxu Zhang, Changjun Wu, Wensheng Huang, Chengshan Xu, Changyong Jin, Yu Wu et al. "Multi-objective optimization design for a double-direction liquid heating system-based Cell-to-Chassis battery module." *International Journal of Heat and Mass Transfer* 183 (2022): 122184. https://doi.org/10.1016/j.ijheatmasstransfer.2021.122184

[7] Mali, Vima, Rajat Saxena, Kundan Kumar, Abul Kalam, and Brijesh Tripathi. "Review on battery thermal management systems for energy-efficient electric vehicles." *Renewable and Sustainable Energy Reviews* 151 (2021): 111611. https://doi.org/10.1016/j.rser.2021.111611

[8] Patel, Jay R., and Manish K. Rathod. "Recent developments in the passive and hybrid thermal management techniques of lithium-ion batteries." *Journal of Power Sources* 480 (2020): 228820. https://doi.org/10.1016/j.jpowsour.2020.228820

[9] Ubale, Divyesh, and Prafulla Ubale. "A critical review on recent developments in battery thermal management system of electric vehicles." *Materials Today: Proceedings* 68 (2022): 2613-2621. https://doi.org/10.1016/j.matpr.2022.09.566

[10] Sharma, Dinesh Kumar, and Aneesh Prabhakar. "A review on air cooled and air centric hybrid thermal management techniques for Li-ion battery packs in electric vehicles." *Journal of Energy Storage* 41 (2021): 102885.

https://doi.org/10.1016/j.est.2021.102885
[11] Kim, Jaewan, Jinwoo Oh, and Hoseong Lee. "Review on battery thermal management system for electric vehicles." *Applied Thermal Engineering* 149 (2019): 192-212. https://doi.org/10.1016/j.applthermaleng.2018.12.020
[12] Zhao, Gang, Xiaolin Wang, Michael Negnevitsky, and Chengjiang Li. "An up-to-date review on the design improvement and optimization of the liquid-cooling battery thermal management system for electric vehicles." *Applied Thermal Engineering* 219 (2023): 119626. https://doi.org/10.1016/j.applthermaleng.2022.119626
[13] He, Liange, Haodong Jing, Yan Zhang, Pengpai Li, and Zihan Gu. "Review of thermal management system for battery electric vehicle." *Journal of Energy Storage* 59 (2023): 106443. https://doi.org/10.1016/j.est.2022.106443
[14] Yu, Zhipeng, Jiakai Zhang, and Weiguo Pan. "A review of battery thermal management systems about heat pipe and phase change materials." *Journal of Energy Storage* 62 (2023): 106827. https://doi.org/10.1016/j.est.2023.106827
[15] Cai, Shaowei, Xuelai Zhang, and Jun Ji. "Recent advances in phase change materials-based battery thermal management systems for electric vehicles." *Journal of Energy Storage* 72 (2023): 108750. https://doi.org/10.1016/j.est.2023.108750
[16] Thawkar, Vivek, and A. S. Dhoble. "A review of thermal management methods for electric vehicle batteries based on heat pipes and PCM." *Journal of the Brazilian Society of Mechanical Sciences and Engineering* 45, no. 2 (2023): 90. https://doi.org/10.1007/s40430-023-04021-3
[17] Thakur, Amrit Kumar, Ravishankar Sathyamurthy, R. Velraj, R. Saidur, A. K. Pandey, Z. Ma, Punit Singh et al. "A state-of-the art review on advancing battery thermal management systems for fast-charging." *Applied Thermal Engineering* 226 (2023): 120303. https://doi.org/10.1016/j.applthermaleng.2023.120303
[18] Hamed, Marwa Mahmoud, A. El-Tayeb, Ibrahim Moukhtar, A. Z. El Dein, and Esam H. Abdelhameed. "A review on recent key technologies of lithium-ion battery thermal management: External cooling systems." *Results in Engineering* 16 (2022): 100703. https://doi.org/10.1016/j.rineng.2022.100703
[19] Youssef, Rekabra, Theodoros Kalogiannis, Hamidreza Behi, Ashkan Pirooz, Joeri Van Mierlo, and Maitane Berecibar. "A comprehensive review of novel cooling techniques and heat transfer coolant mediums investigated for battery thermal management systems in electric vehicles." *Energy Reports* 10 (2023): 1041-1068. https://doi.org/10.1016/j.egyr.2023.07.041
[20] Weragoda, Delika M., Guohong Tian, Arman Burkitbayev, Kin-Hing Lo, and Teng Zhang. "A comprehensive review on heat pipe based battery thermal management systems." *Applied Thermal Engineering* 224 (2023): 120070. https://doi.org/10.1016/j.applthermaleng.2023.120070
[21] Akachi, H. *Structure of a heat pipe.* US Patent No. 4921041, 1990.
[22] Chi, Ri-Guang, Won-Sik Chung, and Seok-Ho Rhi. "Thermal characteristics of an oscillating heat pipe cooling system for electric vehicle li-ion batteries." *Energies* 11, no. 3 (2018): 655. https://doi.org/10.3390/en11030655
[23] Zhao, Xiaohuan, Yue Zhu, and Hailiang Li. "Micro-Channel Oscillating Heat Pipe Energy Conversion Approach of Battery Heat Dissipation Improvement: A Review." *Energies* 15, no. 19 (2022): 7391. https://doi.org/10.3390/en15197391
[24] Chi, Ri-Guang, and Seok-Ho Rhi. "Oscillating heat pipe cooling system of electric vehicle's Li-ion batteries with direct contact bottom cooling mode." *Energies* 12, no. 9 (2019): 1698. https://doi.org/10.3390/en12091698
[25] Zhou, Zhicheng, Yaojie Lv, Jian Qu, Qin Sun, and Dmitrii Grachev. "Performance evaluation of hybrid oscillating heat pipe with carbon nanotube nanofluids for electric vehicle battery cooling." *Applied Thermal Engineering* 196 (2021): 117300. https://doi.org/10.1016/j.applthermaleng.2021.117300
[26] Ling, Yun-Zhi, Xiao-Song Zhang, Feng Wang, and Xiao-Hui She. "Performance study of phase change materials coupled with three-dimensional oscillating heat pipes with different structures for electronic cooling." *Renewable Energy* 154 (2020): 636-649. https://doi.org/10.1016/j.renene.2020.03.008
[27] Zhao, J., X. Zhang, and Z. Rao. "Oscillating heat pipe coupled with phase change material (OHP/PCM) used for battery thermal management." *Journal of Beijing Institute of Technology (English Edition)* 26 (2017): 181-186.
[28] Hongkun, Lu, Noor, M. M., Wenlin, Y., Kadirgama, K., Badruddin, I. A., and Kamangar, S. "Experimental research on heat transfer characteristics of a battery liquid-cooling system with ⊥-shaped oscillating heat pipe under pulsating flow." International Journal of Heat and Mass Transfer 224 (2024): 125363. https://doi.org/10.1016/j.ijheatmasstransfer.2024.125363
[29] Kou, Fangcheng, Xin Wang, Yu Zou, and Jinhan Mo. "Heat transfer performance of the L-shaped flat gravity heat pipe used for zero-carbon heating houses." *Journal of Building Engineering* 76 (2023): 107389. https://doi.org/10.1016/j.jobe.2023.107389
[30] Liu, Xiangdong, Xiaotian Han, Zhaoyu Wang, Guanqiu Hao, Ziwen Zhang, and Yongping Chen. "Application of an anti-gravity oscillating heat pipe on enhancement of waste heat recovery." *Energy Conversion and Management* 205 (2020): 112404. https://doi.org/10.1016/j.enconman.2019.112404
[31] Xu, Chong, Shanglong Xu, Shiteng Wei, and Pengyan Chen. "Experimental investigation of heat transfer for pulsating flow of GOPs-water nanofluid in a microchannel." *International Communications in Heat and Mass Transfer* 110

(2020): 104403. https://doi.org/10.1016/j.icheatmasstransfer.2019.104403
[32] Fumoto, Koji, and Keiko Ishii. "Flat plate pulsating heat pipe operating at ultra-low filling ratio." *Applied Thermal Engineering* 228 (2023): 120468. https://doi.org/10.1016/j.applthermaleng.2023.120468
[33] Czajkowski, Cezary, Andrzej I. Nowak, Agnieszka Ochman, and Sławomir Pietrowicz. "Flower Shaped Oscillating Heat Pipe at the thermosyphon condition: Performance at different rotational speeds, filling ratios, and heat supplies." *Applied Thermal Engineering* 212 (2022): 118540. https://doi.org/10.1016/j.applthermaleng.2022.118540
[34] Yin, D., H. Rajab, and H. B. Ma. "Theoretical analysis of maximum filling ratio in an oscillating heat pipe." *International Journal of Heat and Mass Transfer* 74 (2014): 353-357. https://doi.org/10.1016/j.ijheatmasstransfer.2014.03.018
[35] Zhou, Guoqing, Fengbo Guan, Wenlong Yang, Qin Sun, and Jian Qu. "Start-up and heat transfer characteristics of oscillating heat pipe charged with binary partially miscible organic fluid mixtures." *Applied Thermal Engineering* 231 (2023): 120952. https://doi.org/10.1016/j.applthermaleng.2023.120952
[36] Wei, Aibo, Jian Qu, Huihe Qiu, Cheng Wang, and Gehan Cao. "Heat transfer characteristics of plug-in oscillating heat pipe with binary-fluid mixtures for electric vehicle battery thermal management." *International Journal of Heat and Mass Transfer* 135 (2019): 746-760. https://doi.org/10.1016/j.ijheatmasstransfer.2019.02.021
[37] Barrak, Anwar S., Ahmed A. M. Saleh, and Zainab H. Naji. "An experimental study of using water, methanol, and binary fluids in oscillating heat pipe heat exchanger." *Engineering Science and Technology, an International Journal* 23, no. 2 (2020): 357-364. https://doi.org/10.1016/j.jestch.2019.05.010
[38] Xu, Rongji, Chao Zhang, Hao Chen, Qingping Wu, and Ruixiang Wang. "Heat transfer performance of pulsating heat pipe with zeotropic immiscible binary mixtures." *International Journal of Heat and Mass Transfer* 137 (2019): 31-41. https://doi.org/10.1016/j.ijheatmasstransfer.2019.03.070